Supplementary Information for

Versatile MXene Gels Assisted by Brief and Low-Strength Centrifugation

Weiyan Yu[1,2], Yi Yang[1,2], Yunjing Wang[2], Lulin Hu[1,2], Jingcheng Hao[2,3,]*, Lu Xu[1,2,]* and Weimin Liu[1,2]

[1] State Key Laboratory of Solid Lubrication, Lanzhou Institute of Chemical Physics, Chinese Academy of Sciences, Lanzhou 730000, P. R. China

[2] Shandong Laboratory of Advanced Materials and Green Manufacturing at Yantai, Yantai 264006, P. R. China

[3] Key Laboratory of Colloid and Interface Chemistry & Key Laboratory of Special Aggregated Materials, Shandong University, Jinan 250100, P. R. China

*Corresponding authors. E-mail: jhao@sdu.edu.cn (Jingcheng Hao); xulu@licp.cas.cn (Lu Xu)

Supplementary Figures and Tables

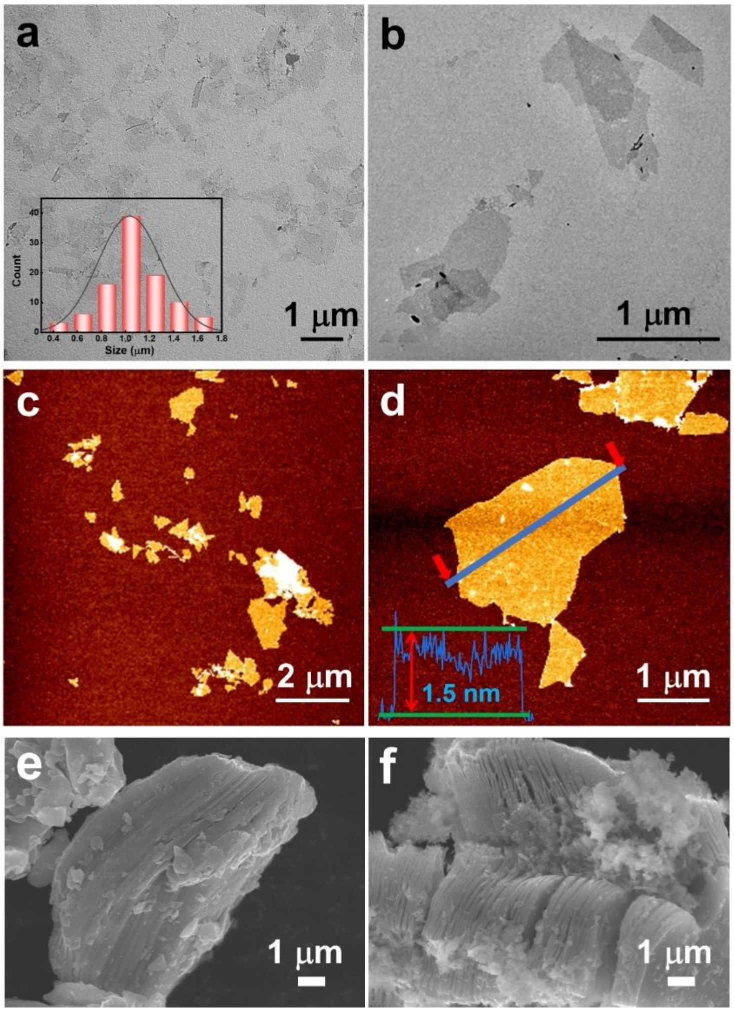

Fig. S1 a, b TEM and **c, d** AFM observations of exfoliated ultrathin $Ti_3C_2T_x$ MXene. SEM images of **e** pristine Ti_3AlC_2 MAX phase and **f** multilayered $Ti_3C_2T_x$ MXene obtained after etching. Insets in **a** and **d** are the particle size distribution and heigh profile of the MXene nanosheets

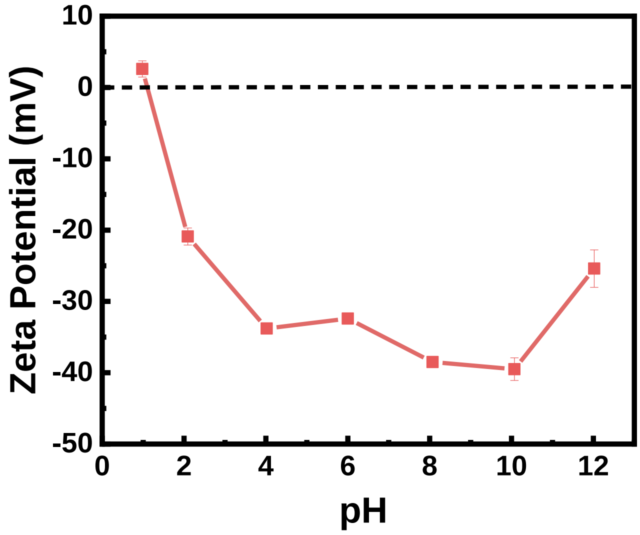

Fig. S2 Zeta potential measurements of $Ti_3C_2T_x$ dispersions at different pH values. T = 25 °C

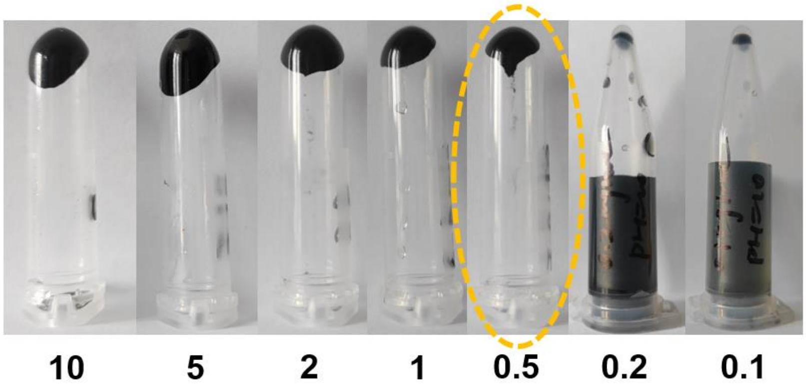

Fig. S3 Photographs of pH 10 $Ti_3C_2T_x$ dispersions at different particle concentrations (in mg mL^{-1}) after centrifugation at 10000 ×g for 30 s. T = 25 °C

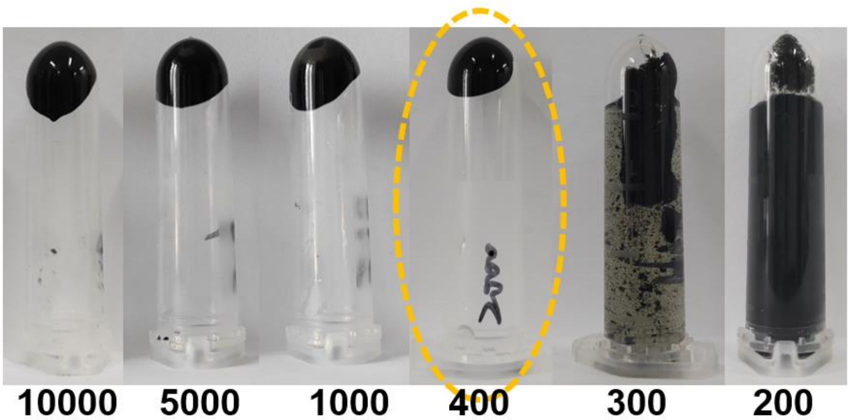

Fig. S4 Photographs of pH 10, 0.5 mg mL^{-1} $Ti_3C_2T_x$ dispersions after exposure to different relative centrifugal forces (RCFs, in ×g) for 30 s. T = 25 °C

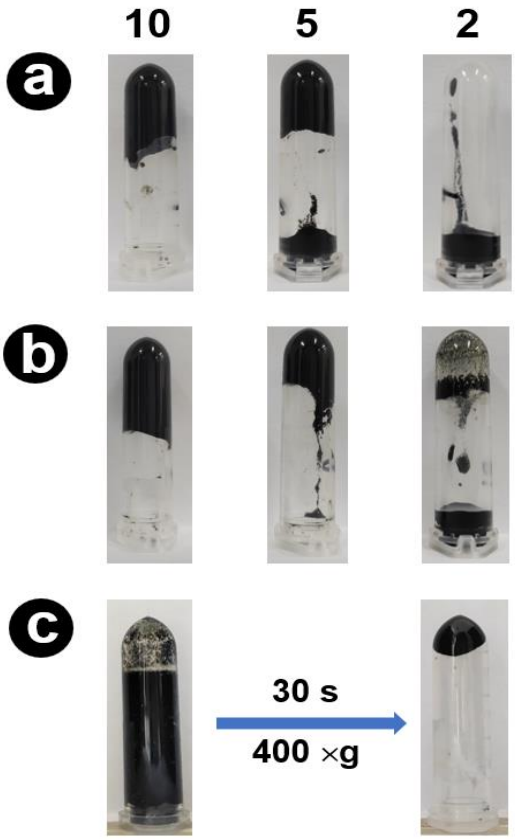

Fig. S5 Photographs of pH 10 $Ti_3C_2T_x$ dispersions at different particle concentrations (in mg mL^{-1}) after addition of **a** Fe^{2+} and **b** Zn^{2+} to a final mass ratio of 3:8 (metal chloride-to-MXene). **c** Photographs of an aqueous dispersion containing 2 mg mL^{-1} $Ti_3C_2T_x$ nanosheets and 5 mmol L^{-1} Fe^{2+} before and after exposure to 400 ×g centrifugation for 30 s. T = 25 °C

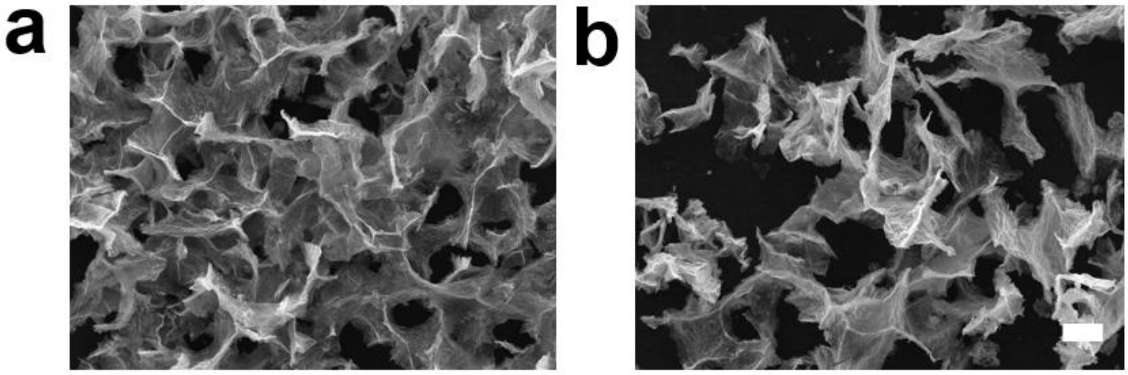

Fig. S6 SEM observations of freeze-dried pH 10 MXene gels **a** and dispersions **b**. Scale bar = 20 µm

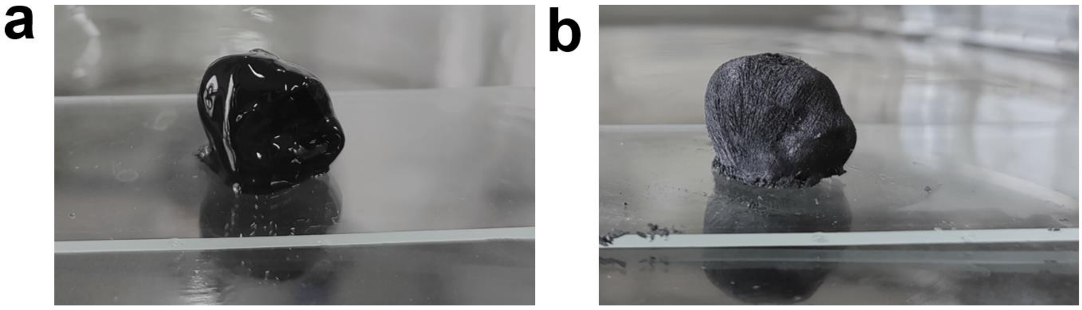

Fig. S7 3D macrostructures of a pH 10 MXene gel **a** before and **b** after complete lyophilization

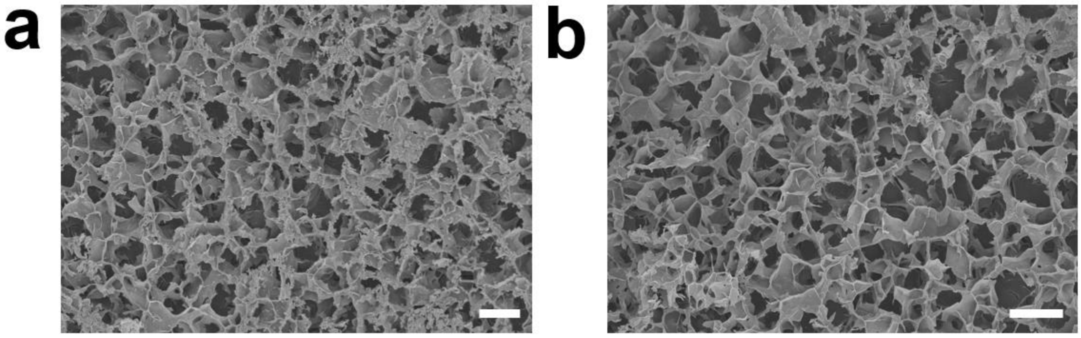

Fig. S8 Cryogenic SEM observations on a pristine pH 10 MXene gel. Scale bar = 5 μm

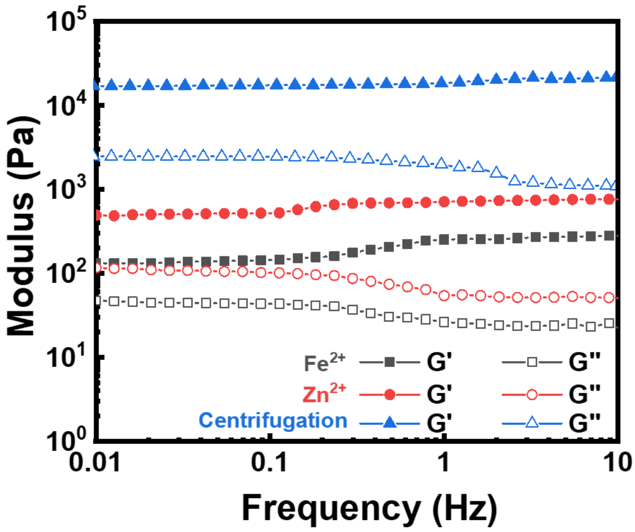

Fig. S9 Comparison in viscoelasticity between the $Ti_3C_2T_x$ gels with an identical water content of ~98 wt% triggered by centrifugation and divalent metal ions. T = 25 °C

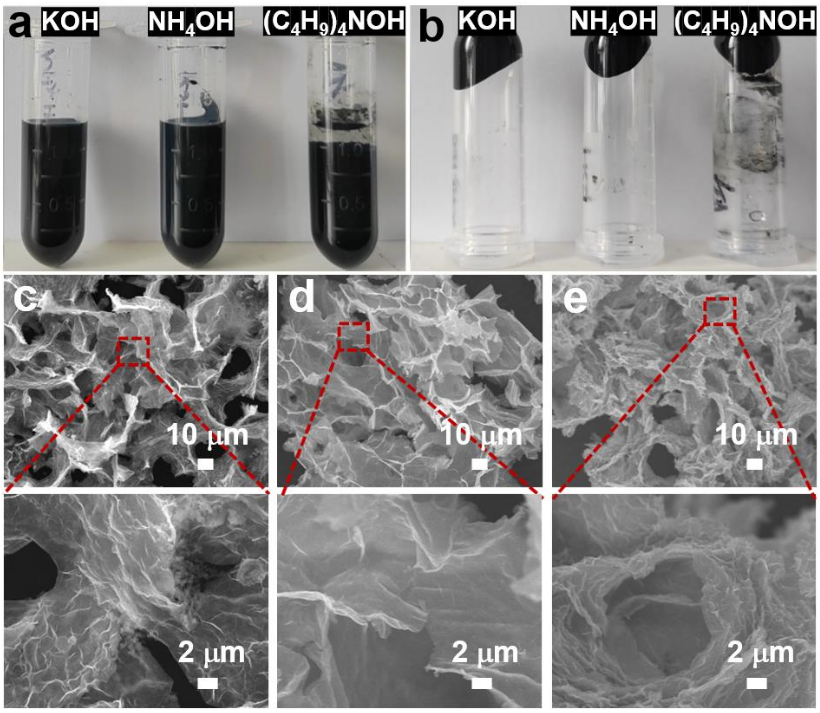

Fig. S10 Photographs of 10 mg mL^{-1}, pH 10 MXene dispersions prepared with different alkalis **a** before and **b** after centrifugation at 400 ×g for 30 s. SEM images of the centrifugation-assisted MXene gels prepared with **c** KOH, **d** NH_4OH and **e** $(C_4H_9)_4NOH$. T = 25 °C

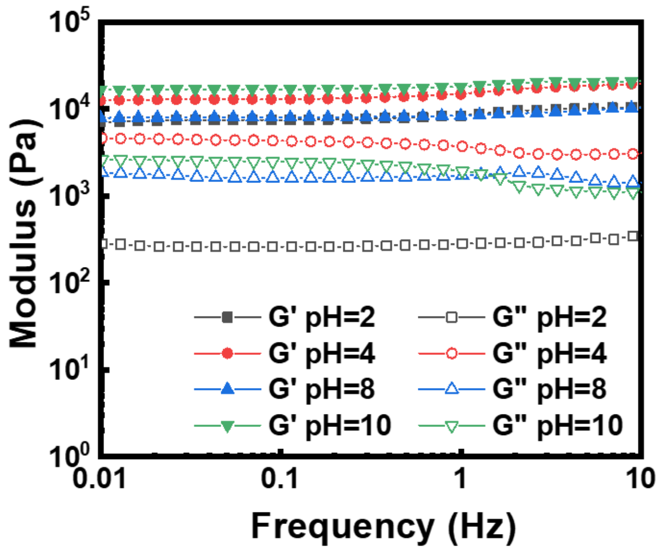

Fig. S11 Rheological property of the centrifugation-assisted MXene gel with different internal pH values. T = 25 °C

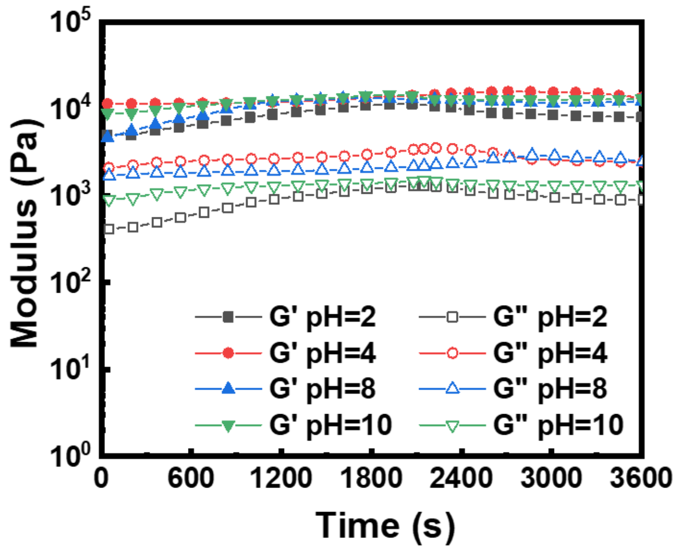

Fig. S12 Changes in viscoelasticity of the MXene gels over time at a constant shear frequency and strain of 1 Hz and 5%, respectively. T = 25 °C

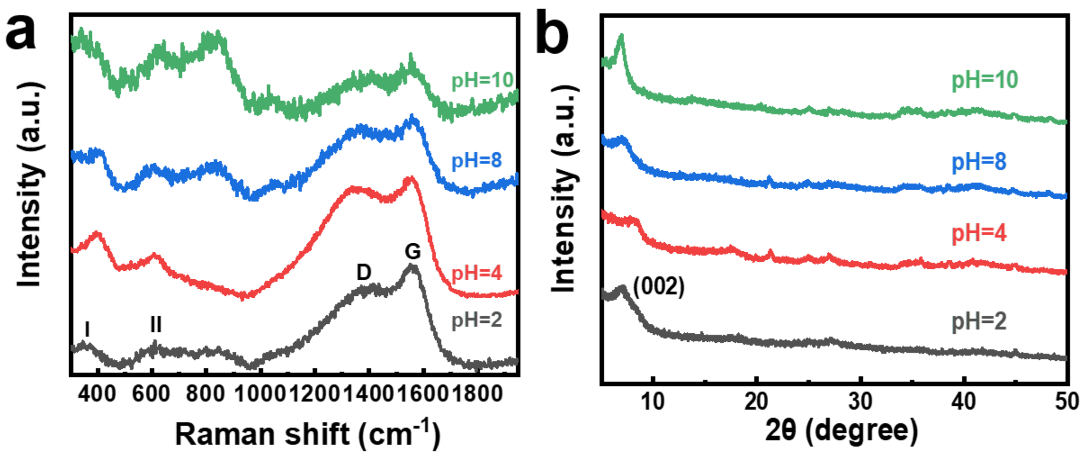

Fig. S13 **a** Raman and **b** XRD profiles of lyophilized MXene gels at different pH values. T = 25 °C

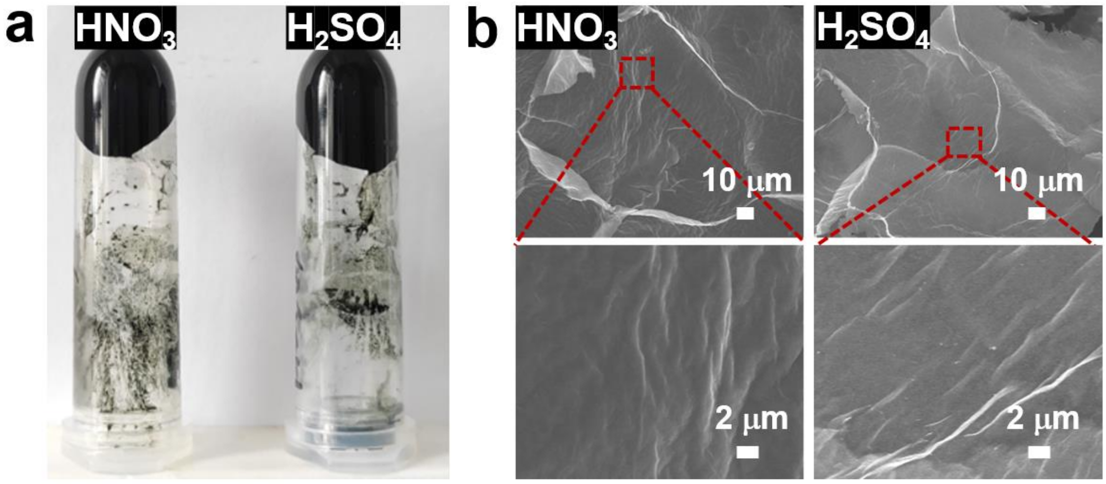

Fig. S14 a Photographs and **b** internal microstructures of pH 2 MXene gels prepared using H_2SO_4 and HNO_3. T = 25 °C

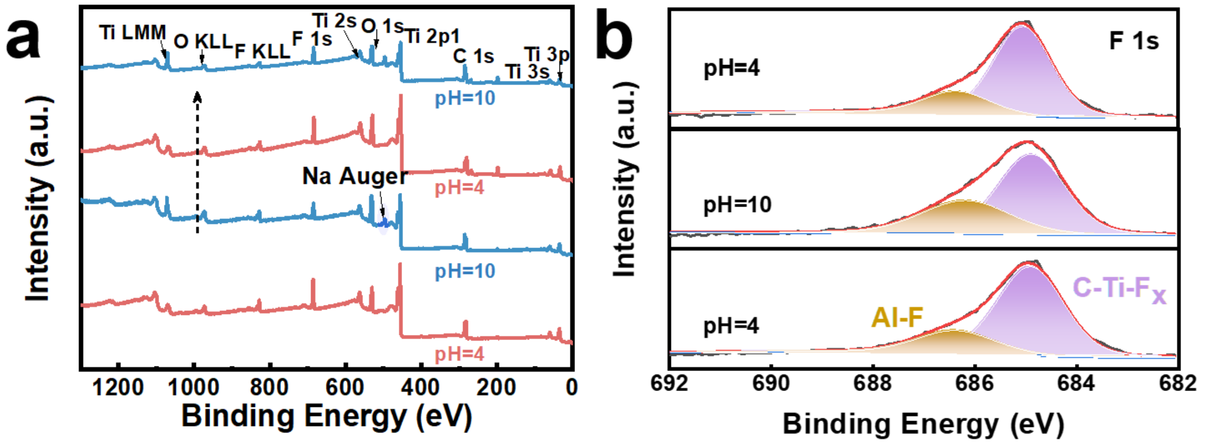

Fig. S15 a Full XPS and **b** XPS F 1s spectra of a lyophilized MXene gel after alternately changing pH between 4 and 10. T = 25 °C

Table S1 Contents of each terminal group determined by the deconvolution and integration of corresponding band areas from the XPS profiles

pH	**-F**	**-O**	**-OH**
pH=4	50.4%	23.9%	25.7%
pH=10	30.3%	48.0%	21.7%
pH=4	48.2%	24.0%	27.8%

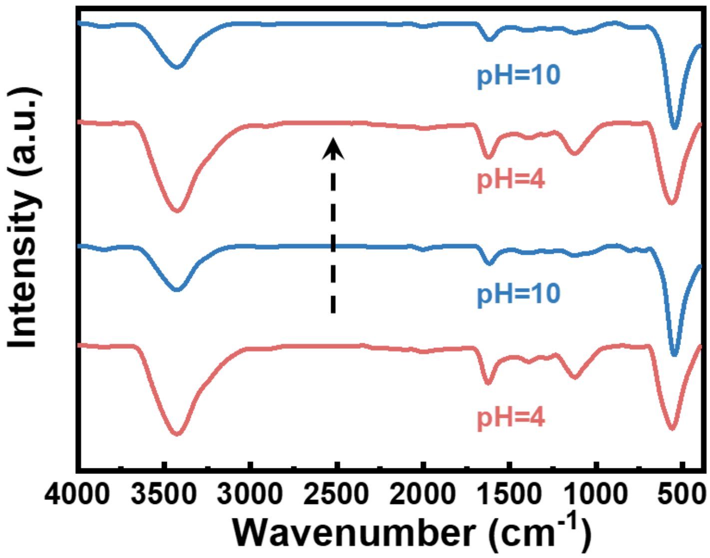

Fig. S16 FTIR profile of a freeze-dried MXene gel after alternately changing its internal pH value between 4 and 10. T = 25 °C

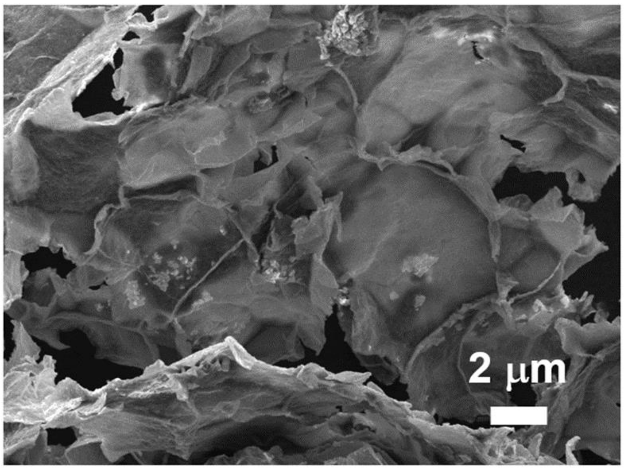

Fig. S17 Internal microstructure of a pH 4 gel after addition of an equal amount of NaCl instead of NaOH

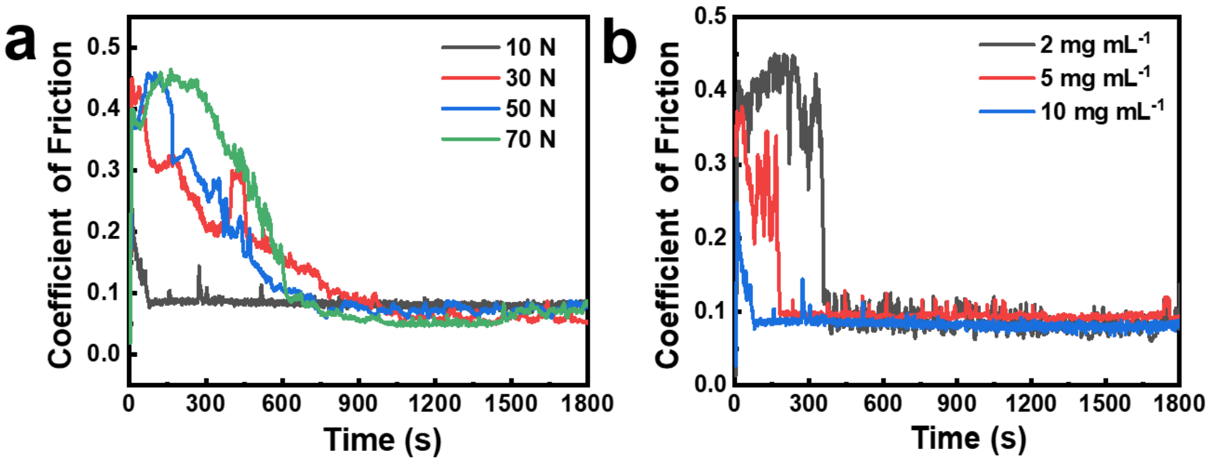

Fig. S18 Effect of **a** applied normal load and **b** initial particle concentration on the CoF of a pH 8 MXene gel. Sliding velocity = 10 mm s^{-1}. T = 25 °C

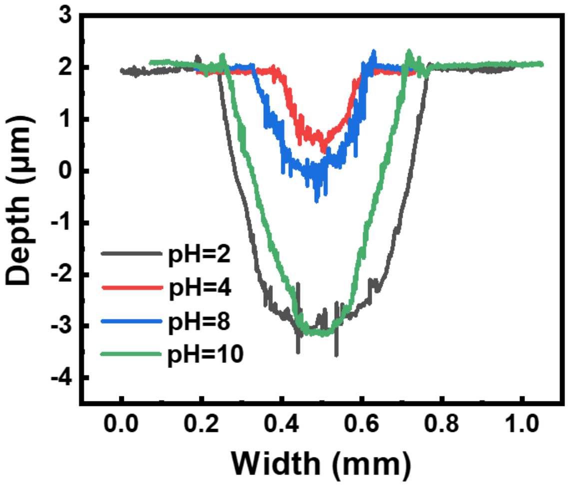

Fig. S19 Width and depth profiles of the wear scar on a steel substrate lubricated with MXene gels in different pH values

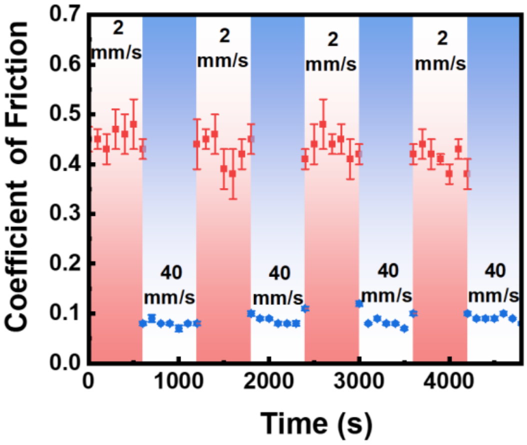

Fig. S20 Variations in the CoF of a pH 4 MXene gel upon alternately changing sliding velocity between 2 and 40 mm s^{-1}. T = 25 °C

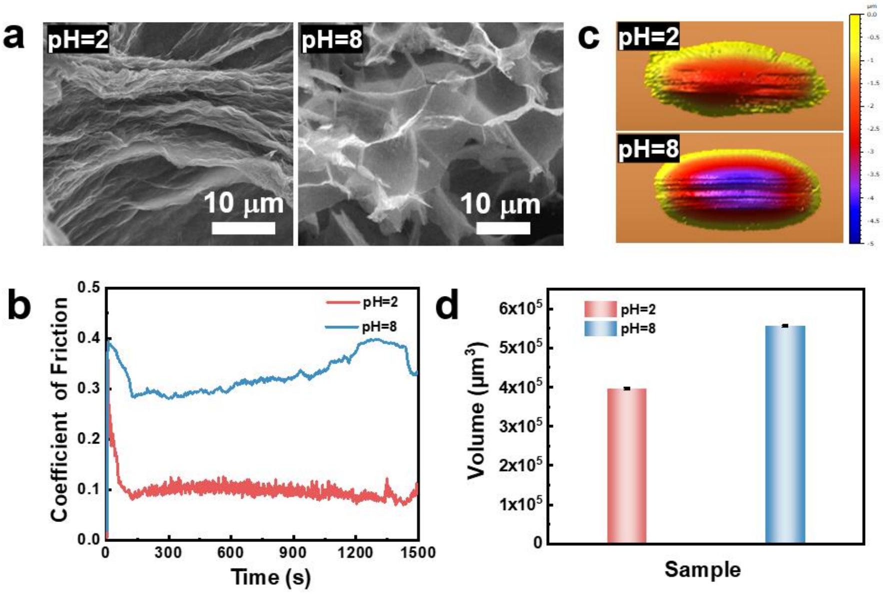

Fig. S21 **a** Internal self-assembled structure and **b** CoF of the MXene-PDDA composite gel at pH 2 and 8. **c** 3D surface topography and **d** abrasive volume of a steel substrate lubricated with the PDDA-containing gel at pH 2 and 8 under 10 N and 10 mm s^{-1}. T = 25 °C

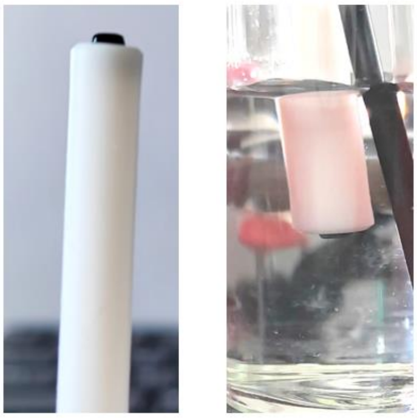

Fig. S22 Photographs of an electrode fabricated with the $Ti_3C_2T_x$ gel

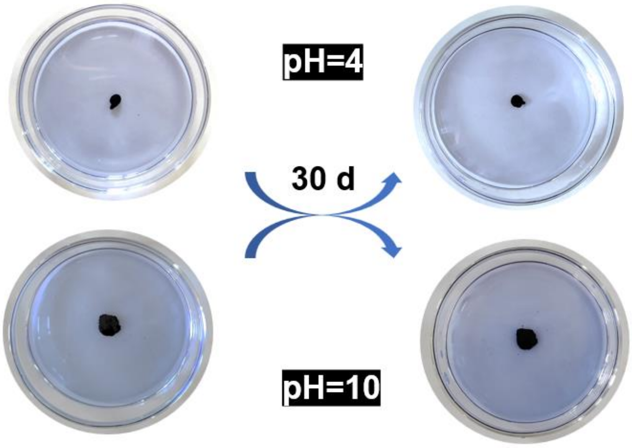

Fig. S23 Photographs of the pH 4 and 10 $Ti_3C_2T_x$ gels after immersed in water reservoirs stained with dye methylene blue for better visualization for 30 days. T = 25 °C

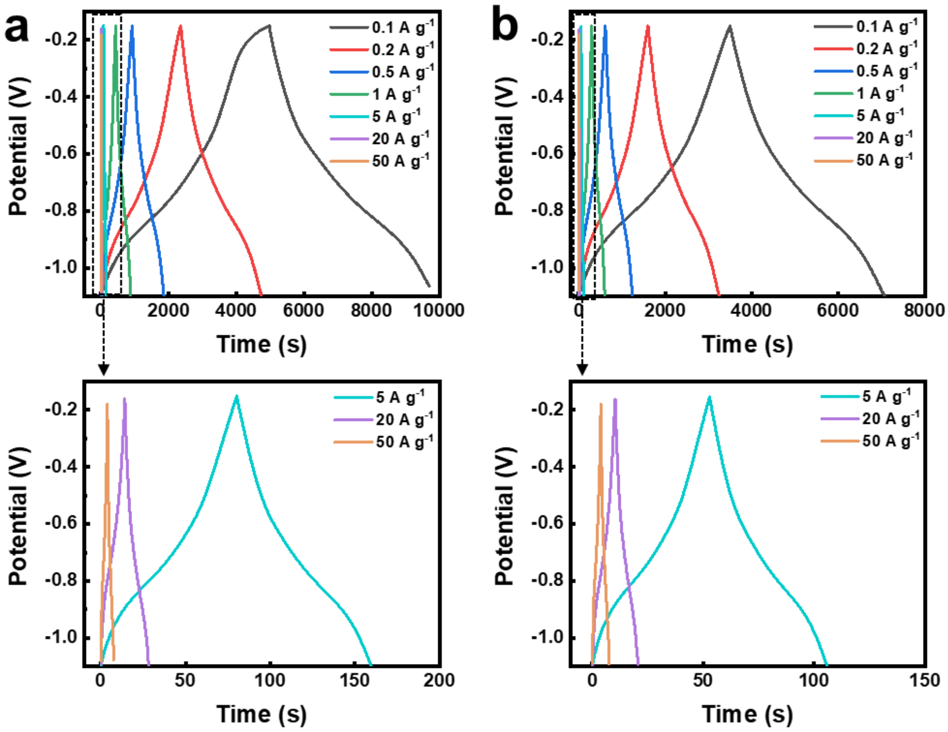

Fig. S24 GCD curves of **a** pH 4 and **b** 10 MXene gels at current densities between 0.1 and 50 A g^{-1}. T = 25 °C

Table S2 Electrochemical performances of the MXene gel-based electrodes reported previously

Gels	Electrolyte	Potential (V)	Specific capacitance (F g^{-1})	Cyclic stability	Refs.
MXene/Fe^{2+}	3 M H_2SO_4	-1.1 to -0.15 (Hg/Hg_2SO_4)	~270 (10 mV s^{-1}) ~255 (100 mV s^{-1})	97.1% after 10,000 cycles	[S1]
MXene/HA	3 M H_2SO_4	-1.1 to -0.15 (Hg/Hg_2SO_4)	~255 (10 mV s^{-1}) ~90 (100 mV s^{-1})	91.7% after 10,000 cycles	[S2]
MXene/H_2SO_4 hydrogel film	3 M H_2SO_4	-1.1 to -0.1 (Hg/Hg_2SO_4)	~375 (10 mV s^{-1})	90% after 10,000 cycles	[S3]
H_2SO_4-thawed MXene	3 M H_2SO_4	-1.2 to -0.2 (Hg/Hg_2SO_4)	~393 (5 mV s^{-1})	95.5% after 10,000 cycles	[S4]
MXene/rGO hydrogel film	3 M H_2SO_4	-1.1 to -0.15 (Hg/Hg_2SO_4)	~300 (10 mV s^{-1}) ~280 (100 mV s^{-1})	94.3% after 10,000 cycles	[S5]
MXene/GO	3 M H_2SO_4	-0.5 to 0.3 (Ag/AgCl)	~470 (10 mV s^{-1}) ~380 (100 mV s^{-1})	~98% after 8,000 cycles	[S6]
MXene/Al^{3+}	1 M H_2SO_4	-0.4 to 0.3 (Ag/AgCl)	~275 (100 mV s^{-1})	~90% after 5,000 cycles	[S7]
MXene/rGO/CNT	3 M H_2SO_4	-0.6 to 0.25 (Ag/AgCl)	~300 (100 mV s^{-1})	97.1% after 10000 cycles	[S8]
Zn^{2+}/MXene hydrogel film	1 M H_2SO_4	-0.6 to 0.2 (Ag/AgCl)	~390 (10 mV s^{-1}) ~350 (100 mV s^{-1})	~98% after 10,000 cycles	[S9]
MXene	3 M H_2SO_4	-1.1 to -0.15 (Hg/Hg_2SO_4)	pH 4: ~635 (5 mV s^{-1}) ~604 (10 mV s^{-1}) ~408 (100 mV s^{-1}) pH 10: ~344 (5 mV s^{-1}) ~322 (10 mV s^{-1}) ~305 (100 mV s^{-1})	pH 4: 85.9% after 10,000 cycles pH 10: 96.7% after 10,000 cycles	This work

Table S3 Electrical conductivity of previously reported MXene-based aerogels

Aerogels	Electrical conductivity (S m^{-1})	Refs.
MXene/CNF	1.8	[S10]
MXene/rGO	695.9	[S11]
MXene/rGO/CNT	9-92	[S8]
MXene/CNF/CNT	2400	[S12]
MXene/polyimide	4	[S13]
MXene/silver nanowire	1532	[S14]
MXene/acidified CNT	447	[S15]
MXene/rGO	36.2	[S16]
MXene	20400 (pH 4) 3800 (pH 10)	This work

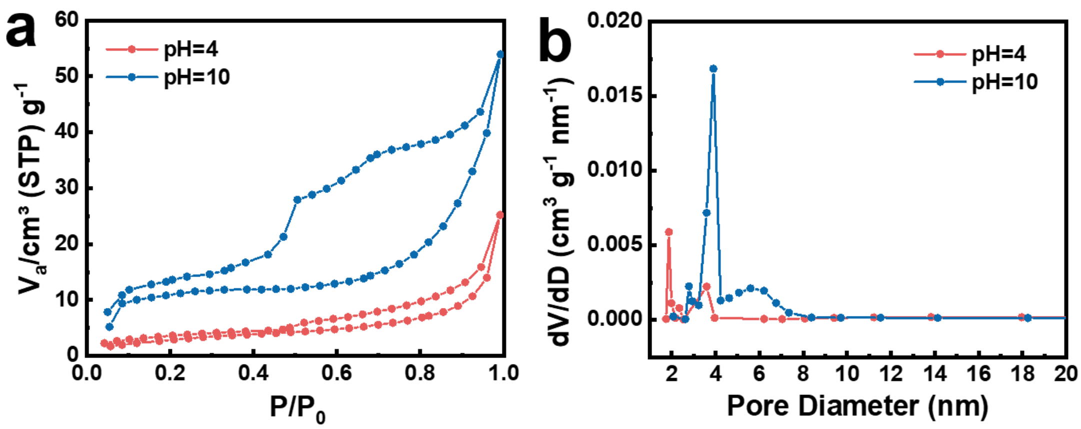

Fig. S25 **a** N_2 adsorption/desorption isotherms and **b** pore size distribution of lyophilized $Ti_3C_2T_x$ gels at 25 °C

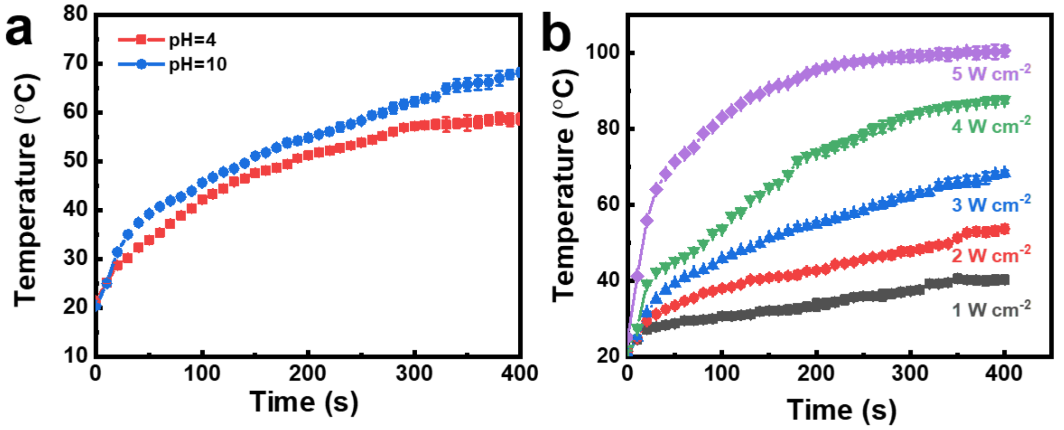

Fig. S26 **a** Temperature variations of the $Ti_3C_2T_x$ gels after irradiated by a 3 W cm^{-2} NIR light for 400 s. **b** Effect of irradiation power on the temperature increment of a pH 10 $Ti_3C_2T_x$ gel. It can be seen that a power above 3 W cm^{-2} would cause a relatively abrupt temperature elevation that may lead to severe water evaporation and changes in the gel properties

Fig. S27 Photograph of the jellyfish-shaped MXene gel coating on a PET substrate in the bending state

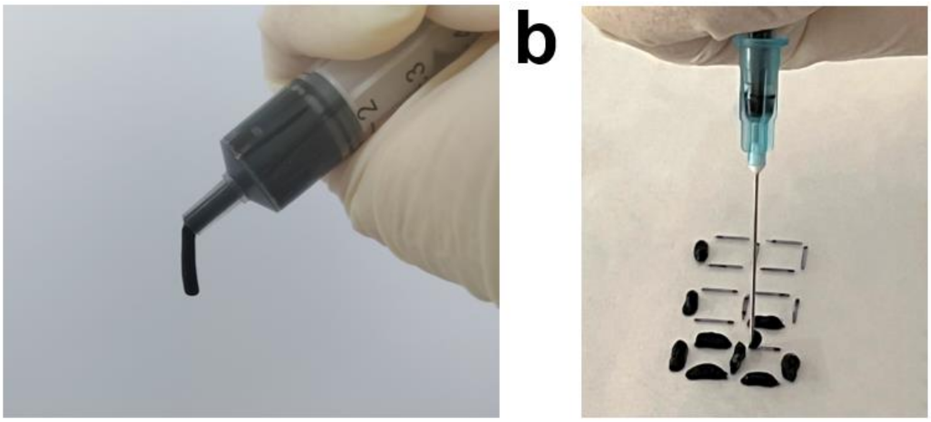

Fig. S28 Photographs of **a** extrusion of the gel through a needle syringe and **b** extrusion-printing of the MXene gel into anti-counterfeiting passwords

Supplementary References

[S1] Y. Deng, T. Shang, Z. Wu, Y. Tao, C. Luo et al., Fast gelation of $Ti_3C_2T_x$ MXene initiated by metal ions. Adv. Mater. **31**, 1902432 (2019). https://doi.org/10.1002/adma.201902432

[S2] Z. Wu, Y. Deng, J. Yu, J. Han, T. Shang et al., Hydroiodic-acid-initiated dense yet porous $Ti_3C_2t_x$ MXene monoliths toward superhigh areal energy storage. Adv. Mater. **35**, e2300580 (2023). https://doi.org/10.1002/adma.202300580

[S3] M.R. Lukatskaya, S. Kota, Z. Lin, M.-Q. Zhao, N. Shpigel et al., Ultra-high-rate pseudocapacitive energy storage in two-dimensional transition metal carbides. Nat. Energy **2**, 17105 (2017). https://doi.org/10.1038/nenergy.2017.105

[S4] X. Huang, J. Huang, D. Yang, P. Wu, A multi-scale structural engineering strategy for high-performance MXene hydrogel supercapacitor electrode. Adv. Sci. **8**, e2101664 (2021). https://doi.org/10.1002/advs.202101664

[S5] Z. Wu, X. Liu, T. Shang, Y. Deng, N. Wang et al., Reassembly of MXene hydrogels into flexible films towards compact and ultrafast supercapacitors. Adv. Funct. Mater. **31**, 2102874 (2021). https://doi.org/10.1002/adfm.202102874

[S6] P. Dutta, A. Sikdar, A. Majumdar, M. Borah, N. Padma et al., Graphene aided gelation of MXene with oxidation protected surface for supercapacitor electrodes with excellent gravimetric performance. Carbon **169**, 225–234 (2020). https://doi.org/10.1016/j.carbon.2020.07.041

[S7] Z. Zhang, Z. Yao, Y. Li, S. Lu, X. Wu et al., Cation-induced Ti3C2Tx MXene hydrogel for capacitive energy storage. Chem. Eng. J. **433**, 134488 (2022). https://doi.org/10.1016/j.cej.2021.134488

[S8] X. Yang, Y. Yao, Q. Wang, K. Zhu, K. Ye et al., 3D macroporous oxidation-resistant $Ti_3C_2T_x$ MXene hybrid hydrogels for enhanced supercapacitive performances with ultralong cycle life. Adv. Funct. Mater. **32**, 2109479 (2022). https://doi.org/10.1002/adfm.202109479

[S9] T. Yun, G.S. Lee, J. Choi, H. Kim, G.G. Yang et al., Multidimensional $Ti_3C_2T_x$ MXene architectures *via* interfacial electrochemical self-assembly. ACS Nano **15**, 10058–10066 (2021). https://doi.org/10.1021/acsnano.1c01727

[S10] N. Wu, Y. Yang, C. Wang, Q. Wu, F. Pan et al., Ultrathin cellulose nanofiber assisted ambient-pressure-dried, ultralight, mechanically robust, multifunctional MXene aerogels. Adv. Mater. **35**, e2207969 (2023). https://doi.org/10.1002/adma.202207969

[S11] S. Zhao, H.-B. Zhang, J.-Q. Luo, Q.-W. Wang, B. Xu et al., Highly electrically conductive three-dimensional $Ti_3C_2T_x$ MXene/reduced graphene oxide hybrid aerogels with excellent electromagnetic interference shielding performances. ACS Nano **12**, 11193–11202 (2018). https://doi.org/10.1021/acsnano.8b05739

[S12] T. Xu, Q. Song, K. Liu, H. Liu, J. Pan et al., Nanocellulose-assisted construction of multifunctional MXene-based aerogels with engineering biomimetic texture for pressure sensor and compressible electrode. Nano-Micro Lett. **15**, 98 (2023). https://doi.org/10.1007/s40820-023-01073-x

[S13] J. Liu, H.-B. Zhang, X. Xie, R. Yang, Z. Liu et al., Multifunctional, superelastic, and lightweight MXene/polyimide aerogels. Small **14**, e1802479 (2018). https://doi.org/10.1002/smll.201802479

[S14] H. Liu, Z. Huang, T. Chen, X. Su, Y. Liu et al., Construction of 3D MXene/Silver nanowires aerogels reinforced polymer composites for extraordinary electromagnetic interference shielding and thermal conductivity. Chem. Eng. J. **427**, 131540 (2022). https://doi.org/10.1016/j.cej.2021.131540

[S15] Z. Deng, P. Tang, X. Wu, H.-B. Zhang, Z.-Z. Yu, Superelastic, ultralight, and conductive $Ti_3C_2T_x$ MXene/acidified carbon nanotube anisotropic aerogels for electromagnetic interference shielding. ACS Appl. Mater. Interfaces **13**, 20539–20547 (2021). https://doi.org/10.1021/acsami.1c02059

[S16] D. Jiang, J. Zhang, S. Qin, Z. Wang, K.A.S. Usman et al., Superelastic $Ti_3C_2T_x$ MXene-based hybrid aerogels for compression-resilient devices. ACS Nano **15**, 5000–5010 (2021). https://doi.org/10.1021/acsnano.0c09959